World Academy of Science, Engineering and Technology
International Journal of Civil and Environmental Engineering
Vol:7, No:2, 2013

Inelastic Strength of Laterally Unsupported Top-Loaded Built-Up Slender Beams

M. Massoud El Sa'adawy, and F. F. F. El Dib

***Abstract*—**Lateral-torsional buckling (LTB) is one of the phenomenae controlling the ultimate bending strength of steel I-beams carrying distributed loads on top flange. Built-up I-sections are used as main beams and distributors. This study investigates the ultimate bending strength of such beams with sections of different classes including slender elements. The nominal strengths of the selected beams are calculated for different unsupported lengths according to the Provisions of the American Institute of Steel Constructions (AISC-LRFD). These calculations are compared with results of a nonlinear inelastic study using accurate FE model for this type of loading. The goal is to investigate the performance of the provisions for the selected sections. Continuous distributed load at the top flange of the beams was applied at the FE model. Imperfections of different values are implemented to the FE model to examine their effect on the LTB of beams at failure, and hence, their effect on the ultimate strength of beams. The study also introduces a procedure for evaluating the performance of the provisions compared with the accurate FEA results of the selected sections. A simplified design procedure is given and recommendations for future code updates are made.

***Keywords*—**Lateral buckling, Top Loading, Ultimate load, Slender Sections.

I. Introduction

THE ultimate bending strength of beams is affected by the Lateral-torsional buckling phenomenon. This phenomenon controls the strength of beams that are not adequately restraint to lateral deflection and twisting out of the loading plane.

For elastic LTB under pure constant bending, the unsupported length is considered to be the beam length (i.e. the beam is laterally restrained at its ends).

The critical buckling moment in the case of pure bending described above is given by [1]:

$$M_{ocr} = \frac{\pi}{L}\sqrt{E I_y G J}\sqrt{1+\frac{\pi^2 E C_w}{G J L^2}} \quad (1)$$

Where L is the length of the beam span which is considered unsupported laterally.

The elastic lateral buckling of beams under vertical loads depends mainly on two parameters: the lateral rigidity of flanges EI_y and the torsional rigidity GJ. For long beams the effect of the lateral rigidity decreases and the torsional rigidity dominates.

For short compact sections the lateral rigidity provides the main resistance of beams. It is noticed that short beams with slender elements are subjected to local failures under heavy vertical loads. The resistance is further reduced by the yield spread either locally or globally due to excessive stresses.

For cases of different moment gradients along the unsupported beam length, the moment gradient factor $\boldsymbol{C_b}$ was used in (1) to take the effect of different moment distribution along the beam's unsupported length [1]:

$$M_{cr} = \frac{C_b \pi}{L}\sqrt{E I_y G J}\sqrt{1+\frac{\pi^2 E C_w}{G J L^2}} \quad (2)$$

The first formula for C_b to find its way into structural design codes is the result of work presented by Salvadori (1955).

There is one omission in either of the two formulas just presented (1), (2). They do not account for the position of the load on the y-axis of the cross-section [1].

AISC-LRFD [2] proposes a linear transition equation from the end of the elastic region to the plastic moment and scales it with *a constant moment gradient factor*, C_b, for all ranges of inelastic beam's slenderness as follows:

$$M_n = C_b\left[M_p - \left(M_p - M_r\right)\left(\frac{L_b - L_p}{L_r - L_p}\right)\right] \le M_p \quad (3)$$

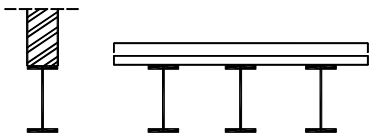

Fig. 1 Free supporting beams

There are different values for C_b in AISC-LRFD depending on the load conditions of the openings. Apart from the load cases mentioned in AISC-LRFD [2], there are some other cases that the transverse loads act away from the shear center axis. For example, top flange loading on a crane runway girder and bottom flange loading acting on a monorail can be considered in practice [3].

M. M. El Sa'adawy, Ph.D, is Associate Professor in Building Research Center, Dept. of Steel Constructions, Cairo, Egypt. (e-mail: m_massoud2002@ yahoo.com).

F. F. F. El Dib, M.Sc., is Ass. Lecturer in Building Research Center, Cairo, Egypt. Dept. of Steel Constructions, (e-mail: farah_fayrouz@yahoo.com).

Beam supporting freestanding walls as well as temporary, or permanent, beam supports of sway free floors, as shown in Fig. 1, are subjected to lateral instability.

Loads on beam top are overturning and thus remarkably reducing the capacity. In the following, these cases are investigated on carefully selected beam sections with various lengths. The cross sections may contain slender webs to reduce material costs. Furthermore, webs are assumed plain with no stiffeners arranged in order to reduce material and labor expenses.

In this paper, all the studied sections are investigated for distributed loading on the center of the top compression flange. This loading case is destabilizing with respect to LTB phenomenon.

The selected sections are symmetric of different classes including slender elements. The beams are simulated using FEA model, including imperfection in the out-of-plane of beam bending.

The purpose of this paper is to investigate the inelastic behavior of LTB for beams loaded on top and built up with slender elements. Taking into consideration the effect of lateral imperfections of the laterally free upper flanges, with parabolic moment gradient along the beam's unsupported span resulted from distributed loading on center of the top compression flange, as to take into consideration factors that affect floor beams flexural behavior and strength.

For this purpose a finite element model based on the software package ANSYS [5] is developed for the nonlinear inelastic LTB analysis of built up I-beams with different slenderness. Then the results are used to investigate the accuracy of the LTB equations given in the AISC-LRFD provisions, and to propose a simplified design procedure.

II. Literature Review

A comprehensive literature review was given by Mohebkhah [3] covering the advances of LTB related research work.

The differential equation of the elastic, on top loaded beam with distributed forces is given as follows [6]:

$$E\,C_M\,\varphi''' - G\,J\,\varphi' - \left[\frac{M^2}{E\,I_y} - M''\,v_M\right]\varphi = 0 \qquad (4)$$

Where M is the bending moment, M'' represent the loading, φ is the rotation and v_M is the distance from loading line of action to the shear center as shown in Fig. 6a.

As for double symmetric I – Beams the center of gravity coincides with the shear center at web mid height. The warping constant is $C_M = I_y \cdot h^2/4$, where h is the height of the beam. GJ is the torsional rigidity, where $J = \sum(bt^3)$. It is noticed that the third coefficient includes M" representing the distributed load acting vertically on the beam and making the mathematical closed solution very complex. The differential equation is solved numerically and the solution is simplified and is given in [6] as follows:

$$M_{CR} = \frac{k}{L}\sqrt{E\,I_y\,G\,J} \qquad (5)$$

In this equation k is given graphically [6] and includes correction factor representing distributed loading on the beam acting on top, at the center of gravity or at the bottom. Equation (5) is used later in this paper to verify the numerical accuracy of the finite element model.

Extensive laboratory tests and numerical investigations have been conducted to study the LTB behavior of steel beams by Nethercot et al., Galambos et al. [1], and Trahair [7]. The findings of the above mentioned studies have led to the developments of modern steel design codes in different parts of the world.

Mohebkhah [3] investigated the nonlinear LTB of inelastic castellated beams under moment gradient using a 3D finite element model and showed that the C_b factors given by AISC-LRFD for the inelastic castellated beams are higher than those obtained using the finite element approach. He also investigated the effects of unbraced length and central off-shear center loading [4] (located at center, top flange and bottom flange) on the moment gradient factor in inelastic behavioral zone.

Grondin and Cheng [8] investigated side sway web buckling of steel beams of laterally supported compression flange numerically and experimentally, including residual stresses and initial imperfection to the numerical model.

Serna et al. [9] proposed a general closed-form expression for determining the equivalent uniform moment factor for any moment distribution and end support conditions, using both finite element analysis and finite difference method.

Choi et al. [10], [11], examined inelastic buckling of discretely braced I-girders by diaphragm bracings and torsional stiffness requirements to attain nominal flexural design strengths, incremental nonlinear finite element analyses considering the initial imperfections and residual stresses are conducted, and the effect of torsional bracing stiffness on inelastic lateral torsional buckling was evaluated. They performed series of experimental test results on the inelastic buckling of torsionally braced I-girder system under uniform bending.

Nguyen et al. [12], [13], presented an analytical solution, as well as FE-analysis for LTB strength and stiffness requirements of I-girders with discrete torsional bracings under a uniform bending condition.

III. Assumptions and Studied Cases

- The material is considered to be idealized perfect elasto-plastic steel.
- The load is acting equally distributed along the top flange.
- The beam is laterally supported only at the ends.
- Flange warping at supports is free.
- Load imperfection is consideredout of web plane.

The considerations of section selections are:

- Sections are widely used in practice.

- Structural element (eg. Web, flanges) dimensions conform to available plate sizes.
- Economical thin web thickness is selected.

The selected section dimensions (mm) are given in Table I.

The beam lengths are varied such that the lateral flange slenderness covers the practical range: L_b/r_T = 30 – 240.

TABLE I
SELECTED SECTIONS

Type	Web Height	Web Thick.	Flange Br.	Flange Thick.
A	300	5	200	14
B	500	5	200	10
C	660	5	200	10

IV. Finite Element Analysis

A. Finite Element Modeling:

The nonlinear computations are performed using the Finite Element Software package [5]. A total of 48 models are simulated for non-linear inelastic static loading for the three selected sections, covering various beam lengths and imperfection values. Both geometric and material nonlinearities are considered in a model. Four side shell elements SHELL 181 are used to model the web, flange (top and bottom) and the end stiffeners. This element considers inelastic big strains with six degrees of freedom at each of its four corners. Flanges and webs are `modeled with about 4cmx4cm divisions, not exceeding aspect ratio of 1:2.

Stiffener plates are used to void the reaction force concentration and local buckling at the beam-ends. Nevertheless, the supporting at each ending is arranged to facilitate the reaction forces gradual transition to the web as shown in Fig. 2. Lateral supports are arranged only at supports providing warping free beam flanges. The supports at the four corners of the beam web are warping-free.

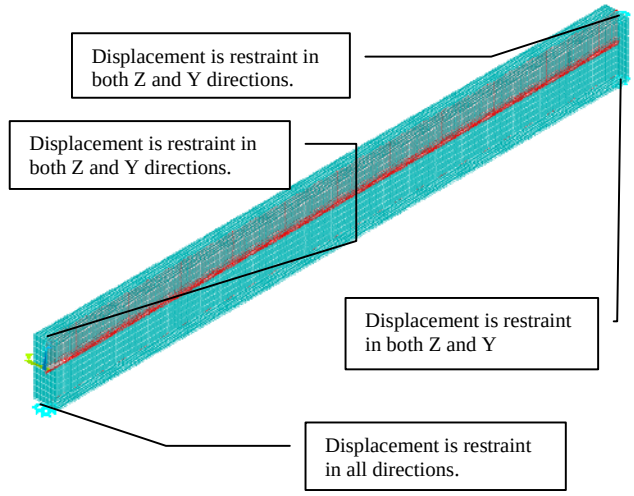

Fig. 2 Model restraints

The steel is modeled as bilinear isotropic material of modulus of elasticity ***E=210,000 Mpa*** till the end of elastic behavior, and ***E=zero Mpa*** at the strain hardening zone. Poissons ratio was set to 0.3. Nominal yield stress ***Fy*** value was specified to be 360 Mpa as typically used for built-up sections.

The iteration procedure selected is the Newton-Raphson method capable of capturing local buckling. Big system deformations are enabled until failure takes place using Von-Mises criteria.

B. Loading of the Model:

Distributed load is applied on the model at the top of the web. The load is increased each step increment until it reaches the value of the ultimate load.

Load imperfections are replaced by small value opposite disturbing horizontal distributed loads applied at upper and lower flanges, as shown in Fig. 3. The value of this disturbing force: $P_H = P \times \frac{e}{h}$, where *h* is the beam height.

The geometric Thus, vertical load is considered to be eccentric loading with respect to the beam centerline by the imperfection value *e*.

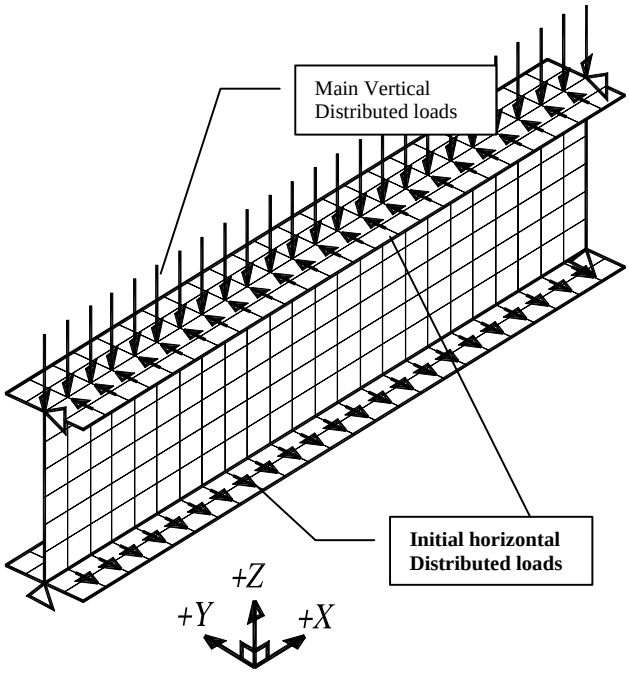

Fig. 3 Loading System

C. Validation of the Finite Element Model:

In order to check accuracy of the finite element solution procedure a comparison is made with the respective results given in [6]. The beam is considered elastic. The Eigen-Value is determined numerically using the Block-Lanczos [5] method. The results are plotted and directly compared to chart [6] relating distributed load position, elastic flexural and torsional rigity, along with the beam length and web height:

$$\chi = \frac{E\ I_y}{G\ J}\left(\frac{h}{2\ L}\right)^2 \quad (6)$$

Then the χ value for each case is compared to the factor k described in (5) as shown in Fig. 4 .

The section type A is used to evaluate critical loads for χ values from near zero until 0.25, which is equivalent to (L_b/r_T) – values from very big (about 400) until 30 respectively. The results are plotted and directly compared to chart .

Good agreement is noticed for χ less than 0.17. At high χ-values beam length become smaller and the system may locally suffer pre-failure due to very high vertical loads. For χ-values less than 0.01, the beam lengths become extremely long and is considered out of the practical range of the lengths used in floor beams. The reference curve [6] provided in Fig. 4 is for loaded top flange. This loading case reduces the flexural resistance of the beam.

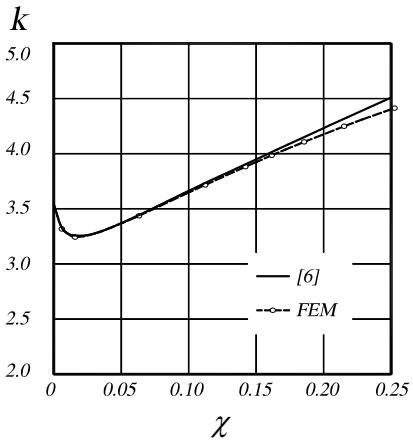

Fig. 4 Comparison with [6]

Hence, it is evident that the FEM results remain in acceptable accuracy under the (L_b/r_T) value range covered by the FEA procedure. Further from this point, FEA is carried out as non-linear inelastic static loading with big deformation to investigate the inelastic behavior of the models for the three selected sections.

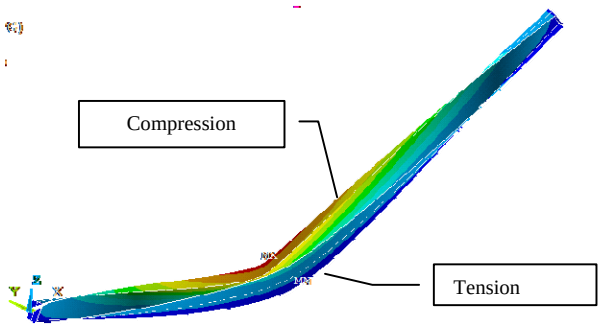

Fig. 5 Excessive Deformations (Post Buckling)

V. Characteristics of Numerical Analysis

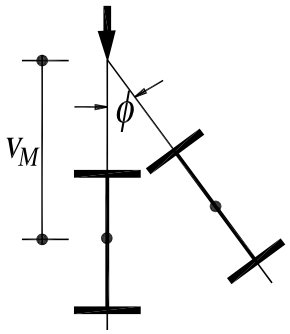

Fig. 6a Section Rotation

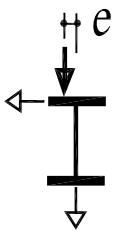

Fig. 6b Displacements

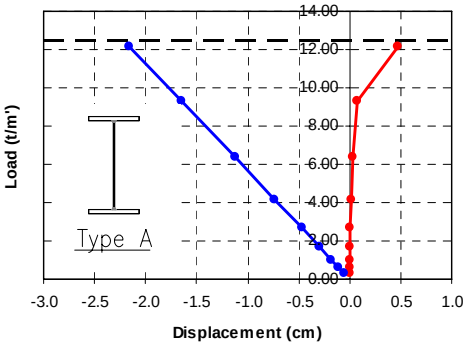

Fig. 6c

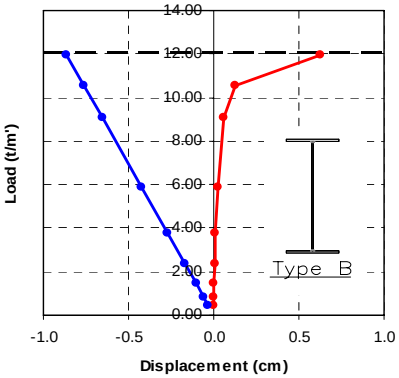

Fig. 6d

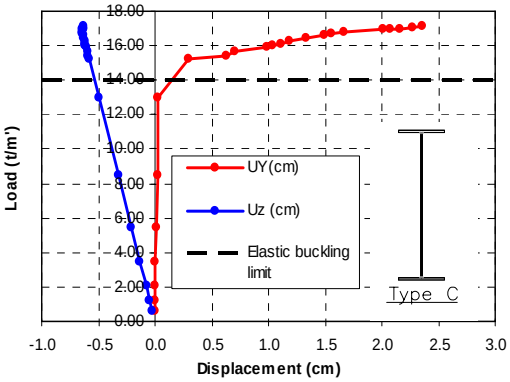

Fig. 6e

The geometrical non-linear inelastic analysis of the model allows for equilibrium under big deformation. It also considers inelastic big strain values. The system may undergo high inelastic deformations and can still accept load increase. The numerically obtained ultimate load may be associated with unrealistic large beam distortions.

For example, the deformed shape shown in Fig. 5 is for beam of section type *A* at (L_b/r_T) value of 220 (L=1216.6 cm). It reached inelastic big strain that cannot be considered as a realistic ultimate load, the ultimate load is rather investigated related to the elastic LTB load, and the means of realistic deformations.

Therefore, for each individual case, every load step was inspected to determine the actual ultimate buckling load.

Spread of yield, excessive stresses and/or deformations, web crippling at mid span below the upper flange, local web shear buckling near supports, and local flange buckling are all potential factors affecting the ultimate lateral buckling load.

The (r_T) values of the selected three sections are around 5cm, hence a constant value section slenderness ratio (L_b/r_T) indicate beam lengths that are approximately the same.

Example load-deflection curves are given in Fig. 6 (d-e): the positive lateral (horizontal) deflection at upper flange as well as the negative vertical deflection of the lower one are plotted with respect to load as in Fig. 6b.

At (L_b/r_T)=80 (L~400cm) - that according to [2] is considered inside the inelastic range of the beam resistance - sections Type A and Type B failure is characterized by sudden failure that doesn't exceed the value of the critical buckling load of the beam buckling load. The lateral displacement of the compression flange (UY) at failure for Type B is slightly greater than that of Type A as shown in Fig. 6c and 6d.

For Type C – that contains slender web – the ultimate load exceeded the value of the elastic beam buckling load with excessive lateral deformations as shown in Fig. 6e (Post Buckling Behavior).

The value of the vertical displacement at failure decreases with the section type: A, B and C respectively. The vertical displacement behavior remains almost linear with the loading increment progression on the beam for all section types.

It should be noted that in all three cases the ultimate load is preceded by big loss of system lateral rigidity ranging from 75% to 95%. This is a strong indication of "The Initial Failure" due to big loss of lateral rigidity.

For higher $\mathbf{L_b/r_T}$ values, the overall lateral deformations at failure are greater than those reached at lower L_b/r_T values to each section of the same type. At failure the members exceeded the elastic critical buckling load by very small values only for section Types B and C .

For L_b/r_T values that are less than 60 – that are resident in plastic zone of the flexural resistance according to [2] – the failure was observed due to shear buckling of the web near support for Type A section.

Crippling of the web plate for Type C is also observed as shown in Fig. 7. Thus, FEA results below L_b/r_T =60 are excluded as they could not be considered representing lateral buckling failure. Examples given in Fig. 6 (c-e) are evaluated considering imperfection ***L/10000***. This value is selected as the ultimate lateral buckling load drops drastically at very small imperfection.

The imperfection sensitivity is checked for the section Type A at L_b/r_T=80 (L=442.4 cm) and its variation is shown in Fig. 8.

For the comparison values shown in Fig. 8, the imperfection value of ***L/1000*** is considered to represent a reasonable value. It gives an acceptable "lower bound" of the ultimate load. For the rest of the analysis both ***L/1000*** and ***L/10000*** imperfection values are investigated for all the selected sections.

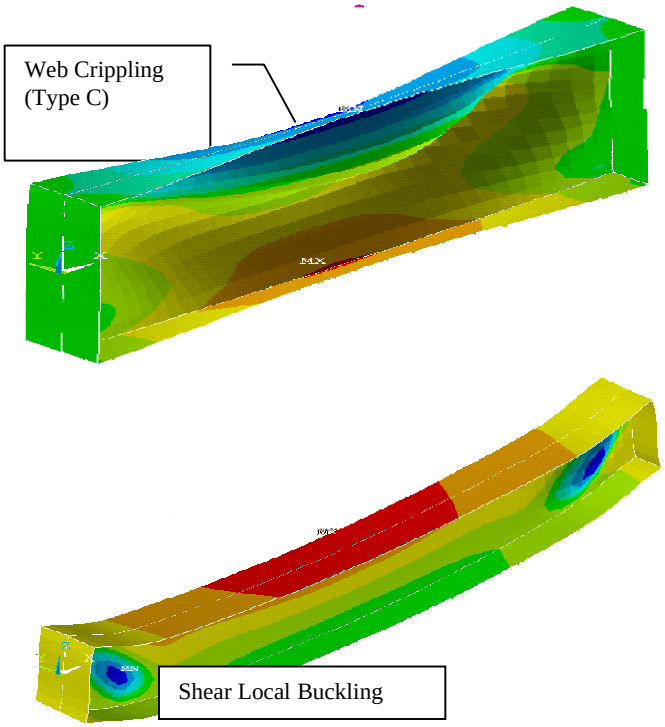

Fig. 7 Crippling and shear local buckling

TABLE II
SECTIONS CLASES

Section Type	Web class	Flange Class	AISC-LRFD [2] Subjection Clause
A	Compact	Non-compact	(F3)
B	Non-compact	Slender	(F4)
C	Non-compact	Slender	(F4)

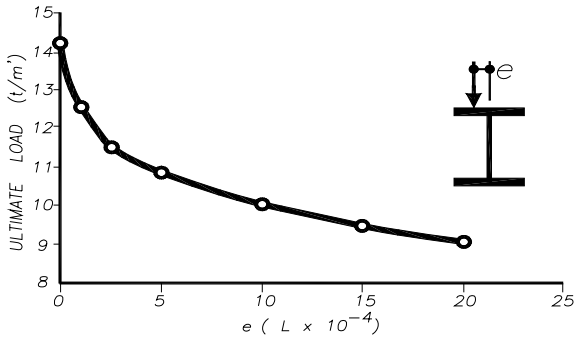

Fig. 8 Imperfection sensitivity

VI. Analytical Solution

A. Comparison of FEA VS AISC-LRFD [2]:

For each Section Type selected, classes are determined according to Table B4.1 of the AISC-LRFD provisions [2], as shown in Table II.

In addition to steel material attributes used in finite element analysis, the flexural resistance of the beams was calculated using C_b value of 1.136 determined for the parabolic gradient moment of the studied case according to (F1-1) in [2].

Each ultimate load value determined by the finite element analysis is converted to the corresponding ultimate bending moment at mid-span, and then divided by the plastic moment of each section. The normalized ratio (M_n/M_p) represents the section flexural capacity.

All the investigated sections developed a flexural strength that is mainly less than the code provisions of the AISC-LRFD [2] as shown in Fig. (9-11). This is also noted for the elastic buckling moment ratio for the same cases.

In Type A section – as shown in Fig. 9 – the imperfection of e = ***L/10000*** represented by the eccentric loading is almost congruent to the elastic buckling curve at the inelastic range.

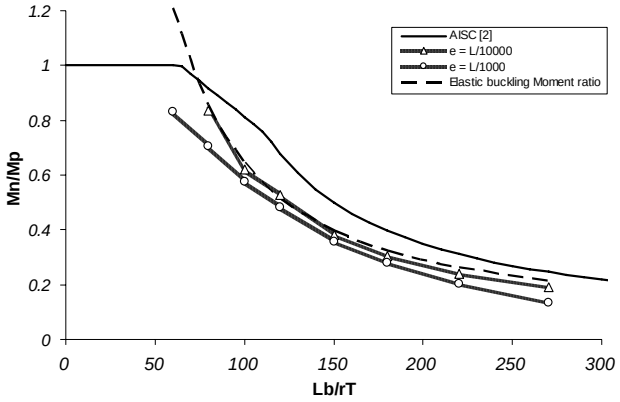

Fig. 9 Flexural Resistance of Type A section

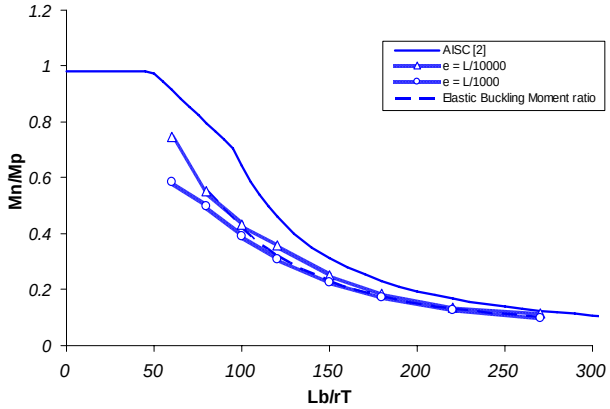

Fig. 10 Flexural Resistance of Type B section

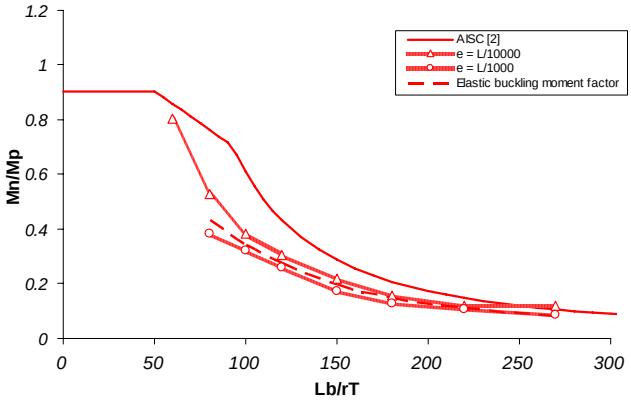

Fig. 11 Flexural Resistance of Type C section

For imperfection e = ***L/1000***, the difference between the nonlinear inelastic capacity and the elastic buckling moment tends to increase at the beginning of the inelastic range and at higher L_b/r_T values. The results of all the performed nonlinear inelastic analysis is upper bounded by the elastic buckling moment values.

In Type B section – as shown in Fig. 11 – the smaller imperfection coincides with the elastic buckling moment curve at higher and lower L_b/r_T values with slight rise at range of L_b/r_T=100~170. The values of the larger imperfection flexural capacity is congruent to the elastic buckling curve at higher L_b/r_T values then begins to drop for $L_b/r_T < 100$.

In Type C section – as shown in Fig. 12 – the section behaves typically as section Type B except that the imperfection of e = ***L/10000*** raises the flexural resistance above the elastic buckling moment resistance for L_b/r_T <170. The post buckling phenomena explains this increase.

B. FE-Ultimate Moment with Respect to Nominal Moment [2]:

Now we can investigate the analytical solution given by the code provisions with respect to accurate behavior of the beams determined by FE analysis. Hence, a procedure is developed to compare the results by means of determining the Finite

Element Ultimate Moment of the selected sections with respect to the assumptions used in the analysis.

M_{FE}/M_n ratios – with respect to AISC-LRFD [2] - are developed for the three sections, for imperfection of e=***L/10000*** as shown in Fig. 13a, as well as for imperfection e=***L/1000*** as shown in Fig. 13b.

The values M_{FE}/M_n are more homogenous for the smaller imperfection value of ***L/10000***, as shown in Fig. 13a. The values are approximately equivalent at the range of L_b/r_T=120~220 with a mean value of 0.78 for this range. The minimum M_{FE}/M_n – ratio occurred at L_b/r_T=100, that is considered at the end of the inelastic range of the flexural resistance for the three sections according to AISC-LRFD [2].

The bigger imperfection of L/1000 resulted in a general reduction and less homogeneity in safety ratios than those of the smaller imperfection. The range of homogeneity remains between L_b/r_T=120 and L_b/r_T=220 with a mean value of 0.68 for this range.

M_{FE}/M_n – ratios decrease with section type for L_b/r_T <120, and vice versa at L_b/r_T >220 out of the above mentioned L_b/r_T range. The factors of safety shows a rise out of the mentioned range for the smaller imperfection ***L/10000***.

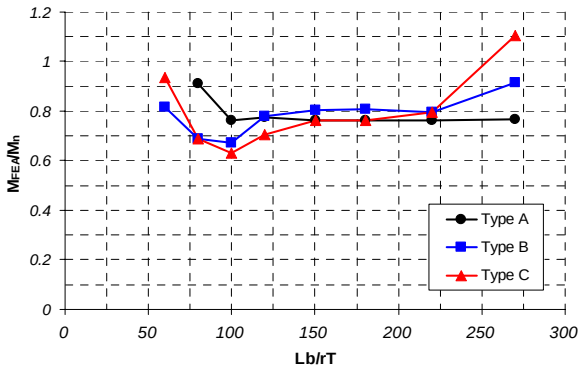

Fig. 13a M_{FE}/M_n – Ratios for e=L/10000 FEA Results

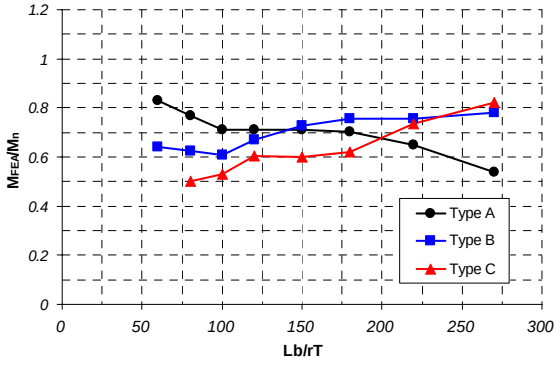

Fig. 13b M_{FE}/M_n – Ratios for e=L/1000

VII. Discussion of Results

The section classes provided by the clause B.4 [2] shows that for a built-up section, the section class is never considered as compact for flexure about strong axis as its compact limit is not available. The section classes for all the selected sections are governed by the flange slenderness according to case 4 of Table B4.1 [2].

The non-compact limit of flange slenderness contains reduction factor K_c [2] that is a function of the web slenderness. Where:

$$k_C = \frac{4}{\sqrt{(h_w / t_w)}} \tag{7}$$

The value of K_c is limited in range between 0.35 and 0.76 [2]. Thus, the web slenderness has a significant effect on the flange class. Hence, the nominal flexural resistance of built–up is affected by the web slenderness value according to the AISC-LRFD [2] provisions.

The comparison of the FEA results to the AISC-LRFD [2] provisions showed that the elastic buckling moment ratios are less than the nominal moment determined using the subjection clauses of (F3) [2] and (F4) [2] for the selected sections in this study. Moreover, the nonlinear inelastic capacities of sections of types B and C exceeded the elastic buckling moment increasingly for lower L_b/r_T. This phenomena is due to the post buckling behavior. This excessive resistance occurred for beams with imperfection of ***L/10000***. Meanwhile, the imperfection of ***L/1000*** resulted in less flexural capacity than the elastic buckling moment for all sections.

By examining the determined ultimate moment values Fig. 9 – 11 along with lateral and vertical deformations Fig. 6. Section Type C developed a flexural capacity that exceeds the elastic buckling moment values for small imperfection value of ***L/10000*** at lower L_b/r_T values. This increase could possibly be due to post buckling behavior and should be investigated extensively in future. Even though the Type B section has the same element class as section Type C, it didn't develop the same load-displacement behavior beyond the elastic buckling limit.

The nonlinear inelastic resistance values - along with the elastic buckling moment ratio - is generally less than the AISC-LRFD [2] provisions nominal resistance. This may be explained by the following reasons:

1) The existence of shear stresses in web increases the web instability, and hence it's ability to support the flange against Lateral-torsional buckling failure. Some cases for very low L_b/r_T values are excluded from the analysis due to shear buckling as in Fig. 7. The Beams are not considered sufficiently stiffened transversely along the whole span according to the traditional assembly of built-up floor beams/ distributors.
2) The load is applied on the top flange, which is a destabilizing load for the cases studied [3] [6].
3) It is agreed that geometric imperfections included in inelastic nonlinear analysis decreases the resistance than that determined by the elastic buckling analysis especially in inelastic zone. Lateral-tortional inelastic buckling is found to be very sensitive to geometrical imperfections. Although the value of ultimate moment exceeded the

elastic buckling at some cases, but they remained under the values determined by the AISC-LRFD [2] provisions.

The existence of shear stresses in web may be considered as the most dominant for the reasons mentioned, as the beam resistance for different moment gradient distributions is mainly related to the pure bending case of constant moment along the unsupported length. Meanwhile, the pure bending case does not contribute shear forces/stresses on the beam section. The effect of shear is effective for the inelastic range approximately at L_b/r_T =60~120 for the selected sections, as short lengths are characterized by high values of loading. The increase in loading for short lengths causes more instability for slender webs for Types B & C, in addition to the large cross-sectional area of the web compared to Type A section.

VIII. Proposal for Code Updates and Recommendations

Recommendations for future code updates shall be based upon the results of the smaller imperfection of L/***1000*** as a conservative selection for the beam flexural resistance.

The results of inelastic zone shall be selected for calibration of the nominal flexural resistance curve of the AISC-LRFD [2] provisions. This is due to the fact that the results provided by this study start approximately at the inelastic zones for the selected sections [2].

Several trials indicated that just a minor modification to the dominating flexural provisions of AISC-LRFD [2] - by using the K_c [2] factor - could be introduced to take account for loading on top flange, section class as well as for geometric imperfection as follows:

1) For Type A section:

Eqn. (F2-2) in [2], to become:

$$M_n = 1.25 k_c \left[M_P - (M_P - 0.7 F_Y . S_X) \frac{(L_b - L_p)}{(L_r - L_p)} \right] . C_b \qquad (8)$$

Eqn. (F2-4) in [2], to become:

$$F_{cr} = 1.25 k_c C_b \frac{\pi^2 . E}{(L_b / r_{ts})^2} . \sqrt{\left(1 + \left(0.078 \frac{J_C}{(S_X . h_0)} \right) . (L_b / r_{ts})^2 \right)} \qquad (9)$$

2) For Type B & C sections:

Eqn. (F4-2) in [2], to become:

$$M_n = 1.25 k_c C_b \left[R_{PC} . M_{YC} - (R_{PC} . M_{YC} - F_L . S_{XC}) \frac{(L_b - L_p)}{(L_r - L_p)} \right] \qquad (10)$$

Eqn. (F4-5) in [2], to become:

$$F_{cr} = 1.25 k_c C_b \frac{\pi^2 . E}{(L_b / r_T)^2} . \sqrt{\left(1 + \left(0.078 \frac{J_C}{(S_X . h_0)} \right) . (L_b / r_T)^2 \right)} \qquad (11)$$

The efficiency of the proposed modification with respect to the flexural capacities using the same algorithm of the AISC-LRFD [2] is shown in Fig. 14 (a, b).

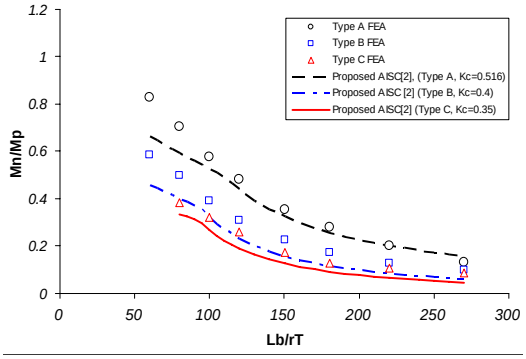

Fig. 14a Proposal compared to L/1000 FEA Results

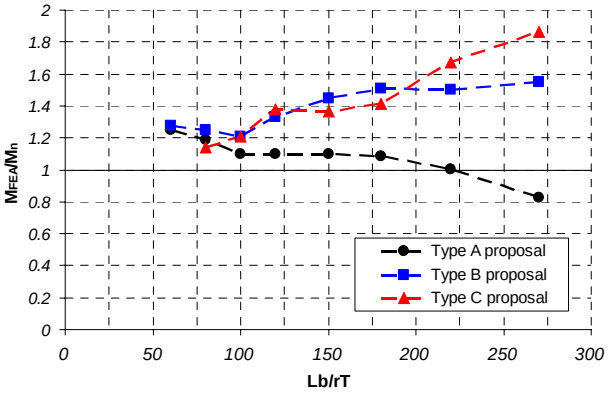

Fig. 14b M_{FE}/M_n – Ratios of the proposal. According to (8) to (11)

The comparison shows improved M_{FE}/M_n - ratio for the studied slender sections of types B & C, that increases with higher L_b/r_T values most likely to be used with their depths. For Type A section, the ratio drops under 1 at approximately L_b/r_T=220 that is considered the end of the practical range of the study. Further more, non-compact sections of Type A section have the smallest height and thus are not likely to be used with long beams.

The proposed modifications could be used under the following conditions:

1) The L_b/r_T range of application shall be between 60 and 220, such that the web height remains in the practical range of usage. As for beams in L_b/r_T < 60 deep beam theory may be sounder to be used in addition to careful investigation of shear- and/or local buckling phenomenae as in Fig. 7.
2) In case no adequate- and/or enough rigid lateral supporting of the compression upper flange. The designer should determine the out-of-plane supporting condition of the beam compression flange.

The following recommendations could be made:

1) Residual stresses, and their effect on the beam flexural capacity should be accounted for. Further capacity reduction is expected.
2) Post-buckling behavior of lateral-torsional buckling, especially for slender sections, should be investigated.
3) Local-, shear- buckling and/or crippling are crucial in short beams. Their interaction should be investigated.
4) Loading positions, with different moment gradients along the unsupported length, need more investigations as the analytical solution may differ from case to another.

IX. Conclusions

Investigated beams are loaded on top and considered laterally unsupported. They have built up sections with economical thin webs. The top loading in addition to a very small lateral imperfection ***L/10000*** reduced the ultimate load remarkably. A lateral imperfection of ***L/1000*** is conservatively selected to obtain ultimate loads that are under the upper bound for the ultimate load (The elastic critical buckling load). Nevertheless, the beams behaved differently with respect to the flange lateral slenderness L_b / r_T:

As for small slenderness, different failure types are found: Local- and/or web shear buckling, web crippling under vertical load side by side with lateral buckling failure are determined. These failure types are associated with large local and/or lateral deformations. Such short beams should be carefully checked for all possible failure cases.

Beams with medium values of slenderness L_b/r_T=60-120 failed mainly due to lateral instability associated with reasonable global deformations. Their corresponding ultimate load is remarkably reduced by up to 40% compared to code provisions. This reduction could be accounted for by introducing a simplified factor in the related code provisions of the AISC-LRFD [2], which is valid for similar cases in the given slenderness range and is proven to be accurate enough.

Very long beams failed in case of ***L/10000*** imperfection due to excessive big deformations. Failure loads exceeded the Elastic Euler Buckling Load and post buckling failure type dominated. Prior to the failure stage, a huge reduction in the lateral system rigidity is yet noted near the elastic buckling load (up to 90%). This may be called "The Initial Failure" due to lateral buckling. This initial failure load should always be considered to determine a reasonable ultimate load.

References

[1] T.V. Galambos, A.E. Surovek "Structural Stability of Steel: Concepts and Applications for structural engineers". P*ublished by John Wiley & Sons, Inc., Hoboken*, New Jersey,2008.
[2] AISC-LRFD, "Specification for structural steel buildings (AISC-LRFD 360-05)". Chicago (IL): *American Institute of Steel Construction*, March 9, 2005.
[3] A. Mohebkhah, "Lateral buckling resistance of inelastic I-beams under off-
shear center loading", *Thin-Walled Structures*, 2011; 49:431–436.
[4] A. Mohebkhah," The moment-gradient factor in lateral-torsional buckling on inelastic castellated beams". *Journal of Constructional Steel Research*,
2004;60: 1481–94.
[5] ANSYS, " User's manual, version 5.4". *ANSYS Inc.* 201Johnson Road, Houston, PA, 15342-1300. 1998.
[6] C.F. Kollbrunner, M. Meister, "Knicken, Biegedrillknicken, Kippen , Theorie und berechnung von Knickstaeben, Knickvorschriften". *Published by Springer Verlag*, 1961.
[7] NS. Trahair, " Flexural-torsional buckling of structures". *Boca Raton. London: E&FN Spon*. 1993.
[8] G Y Grondin, J J R Cheng , "Sidesway Web Buckling of Steel Beams". *Engineering Journal*, 1999(fourth Quarter): 169-179
[9] Serna et al., "Equivalent uniform moment factors for lateral–torsional buckling of steel members". *Journal of Constructional Steel Research 2006;62:566–580.*
[10] Choi et al., " Inelastic buckling of torsionally braced I-girders under uniform bending" I. Numerical parametric studies. *Journal of constructional Steel Research*, 2010;66:304-316.
[11] Choi et al, " Inelastic buckling of torsionally braced I-girders under uniform bending", II:Experimental study. *Journal of Constructional Steel Research*, 2010;66:1128-1137.
[12] Nguyen et al., " Lateral_torsional buckling of I-girders with discrete torsional bracings". *Journal of Constructional Steel Research*, 2010;66:170-177.
[13] Nguyen et al. , "Flexural-torsional buckling strength of I-girders with discrete torsional braces under various loading conditions". *Engineering Structures* , 2012; 36: 337–350.